# Calculation of equatorial currents

by Yu. L. Demin[1] and A. S. Sarkisyan[1,2]

## 1. Introduction

Many calculations of the stationary and seasonal currents in the nonequatorial regions of the oceans have been done using an earlier model published by Sarkisyan (1969). The references list several new publications in this series (Bulatov *et al.*; Demin, 1975). The detailed analysis and survey of the diagnostic calculations were published recently in English (Sarkisyan, 1977). These investigations show the efficiency of the method and make some improvement in the calculation technique. The model allows us to take into account the nonlinear terms and effect of the horizontal viscosity only when these effects are sufficiently small (Sarkisyan and Pastuchov, 1970; Seidov, 1975).

At the equatorial belt, this model is not applicable because the nonlinear terms are larger. The calculations show that the width of this belt is about 4-5° (Holland and Hirschman, 1972; Demin and Sarkisyan, 1974). For this region we propose another calculation method based on the work of Sarkisyan (1970). Some preliminary calculations using this model were performed by the authors (Sarkisyan and Serebryakov, 1974; Demin, 1975b).

The calculations of the currents for both hemispheres are performed in two stages. a) First, we calculate the large-scale currents of both hemispheres using the linear quasi-geostrophic model, omitting the local details of the equatorial currents; in this stage there are no grid points at the equator itself. For example, the points nearest to the equator are situated at 2.5°N and 2.5°S if the grid mesh equals 5°. b) We consider the equatorial belt where calculations must be made with high accuracy. In the northern and southern liquid boundaries of this belt, the current velocities are specified from quasi-geostrophic large-scale calculations, the nonslip boundary conditions are given on the solid side boundaries. In the equatorial belt, all the nonlinear terms and horizontal viscosity effects are taken into account. These two regions overlap each other, resulting in a feedback effect of equatorial currents on the surrounding regions.

1. Institute of Oceanology, USSR Academy of Sciences, 1, Letnaya, Moscow j-387, USSR.

2. In part supported by Geophysical Fluid Dynamics Laboratory/NOAA and by The Geophysical Fluid Dynamics Program/Princeton University.

## 2. The statement of the problem and the calculation methods

Let us consider a narrow equatorial belt with arbitrary bottom relief and side boundaries. The three-dimensional stationary density field in this basin, as well as the wind stress, is specified from observed data. Our problem is to calculate the current velocities in this basin. The basic system of hydrodynamic equations is as follows:

$$u\frac{\partial u}{\partial x}+v\frac{\partial u}{\partial y}+w\frac{\partial u}{\partial z}-fv=-\frac{1}{\rho_0}\frac{\partial P}{\partial x}+\frac{\partial}{\partial z}\nu\frac{\partial u}{\partial z}+A_l\nabla^2 u\,, \tag{1}$$

$$u\frac{\partial v}{\partial x}+v\frac{\partial v}{\partial y}+w\frac{\partial v}{\partial z}+fu=-\frac{1}{\rho_0}\frac{\partial P}{\partial y}+\frac{\partial}{\partial z}\nu\frac{\partial v}{\partial z}+A_l\nabla^2 v\,, \tag{2}$$

$$P=\rho_0 g\zeta+g\int_0^z \rho' d\xi\,, \tag{3}$$

$$\frac{\partial u}{\partial x}+\frac{\partial v}{\partial y}+\frac{\partial w}{\partial z}=0, \tag{4}$$

where $u$, $v$, $w$ are current velocity components along the $x$, $y$, $z$ axes respectively. The axis $x$ is directed eastward, $y$—northward, $z$—vertically downward. The center of the coordinate system is situated on the undisturbed sea surface, $f=2\omega\sin(y/R)$ is the Coriolis parameter, where $R$ is the radius of the earth; $P$, $\rho'$ are the anomalies of pressure and density; $\rho_0$ is the maximal value of the density; $\zeta=\zeta_1+\frac{P_a}{\rho_0 g}$, where $\zeta_1$ is the physical sea surface level, and $\zeta$ is the relative surface level. $P_a$ is the atmospheric pressure on the sea surface, $A_l$, $\nu$ are the coefficients of horizontal and vertical turbulent viscosity, $\nabla^2=\frac{\partial^2}{\partial x^2}+\frac{\partial^2}{\partial y^2}$.

The boundary conditions are as follows. On the sea surface wind stress is known and the "rigid lid" condition is given ($w$=0). On the ocean bottom the nonslip conditions for all of the velocity components are taken. The horizontal components of the current velocity are specified on the liquid side boundaries, and are equal to zero on the solid sides.

The above mentioned four equations contain five unknown functions $u$, $v$, $w$, $P$ and $\zeta$ ($\rho$ is specified). We use the above mentioned additional boundary condition for $w$ and construct an equation for $\zeta$. For this reason we integrate the equations (1) and (2) by $z$ from 0 to ocean bottom $H$, then differentiate the first by $x$ and the second by $y$, then add these two equations to each other. We use the listed equations (3) and (4) and after some simple transformations receive the equation

$$\underbrace{\nabla^2\zeta}_{\text{I}}+\underbrace{\frac{1}{H}\frac{\partial H}{\partial x}\frac{\partial\zeta}{\partial x}+\frac{1}{H}\frac{\partial H}{\partial y}\frac{\partial\zeta}{\partial y}}_{\text{II}}$$

$$= \underbrace{-\frac{1}{\rho_0 H}\int_0^H (H-z)\,\nabla^2\rho'\,dz}_{\text{I}} \underbrace{-\frac{1}{\rho_0 H}\left(\frac{\partial H}{\partial x}\int_0^H \frac{\partial \rho'}{\partial x}\,dz + \frac{\partial H}{\partial y}\int_0^H \frac{\partial \rho'}{\partial y}\,dz\right)}_{\text{II}}$$

$$+ \underbrace{\frac{\vec{div\tau}}{\rho_0 gH}}_{\text{III}} \underbrace{-\frac{1}{gH}\int_0^H \left(\frac{\partial^2 u^2}{\partial x^2} + 2\frac{\partial^2 uv}{\partial x \partial y} + \frac{\partial^2 v^2}{\partial y^2}\right) dz}_{\text{IV}}$$

$$\underbrace{+\frac{f}{gH}\int_0^H \left(\frac{\partial v}{\partial x} - \frac{\partial u}{\partial y}\right) dz}_{\text{V}}$$

$$\underbrace{-\frac{\beta}{gH}\int_0^H u\,dz}_{\text{VI}} + \underbrace{\frac{\vec{div\tau}^{(H)}}{\rho_0 gH}}_{\text{VII}} + \underbrace{\frac{A_l}{gH}\left(\frac{\partial H}{\partial x}\nabla^2 u|_{z=H} + \frac{\partial H}{\partial y}\nabla^2 v|_{z=H} - \nabla^2 w|_{z=H}\right)}$$

(5)

where $\tau_x$, $\tau_y$ are the components of the wind stress, $\tau_x^{(H)} = \rho_0\left(\nu\,\frac{\partial u}{\partial z}\right)_{|z=H}$, $\tau_y^{(H)} = \rho_0\left(\nu\,\frac{\partial v}{\partial z}\right)_{|z=H}$ the components of the bottom stress, $\beta = \frac{df}{dy}$. A scale analysis reveals that the main terms of equation (5) are the terms of Group I, generated by pressure anomalies in the ocean. On the left side of this equation the terms of Group I represent the effect of sea surface topography, and on the right side, the integral of the pure baroclinic part of the pressure anomaly.

We emphasize the principal difference between equation (5) and its counterpart in a quasi-geostrophic model. In a quasi-geostrophic model, we treat an equation for vorticity, but (5) is an equation of divergence. In vorticity equations the nonlinear terms would be dominant at the equator. In equation (5) we impose the pressure gradient (the terms of Group I) to the nonlinear terms, and it aids in constructing a stable finite difference scheme for $\zeta$. In equation (5), the $\beta$ effect, (the term VI) is not the dominant one, it is smaller than the terms of Group I and makes it possible to keep this term on the right side of equation (5) and take it into account using a method of successive approximations. Finally, it is possible that in middle and high latitudes where $f$ is large enough, equation (5) will not be convenient for numerical calculations because Group V is too large.

We turn now to boundary conditions for the function $\zeta$. Generally, we have to construct the relations for the calculation of $\zeta$ on all boundary lines, but the northern and southern liquid boundaries are in the region of geostrophic balance, where all the characteristics, including $\zeta$ were calculated by the quasi-geostrophic model. We have only to calculate this function on the solid (eastern and western) side boundaries. Because of the nonslip boundary condition on the side boundaries we have

$$u = v = 0 \tag{6}$$

If the side boundaries are vertical, the vertical derivatives of $u$ and $v$ are also equal to zero.

Taking into account these simplifications, we integrate equation (2) by $z$ from 0 to ocean bottom $H$ and for the meridional part of the boundary very easily derive

$$\frac{\partial \zeta}{\partial y} = -\frac{1}{\rho_0 H}\int_0^H (H-z)\,\frac{\partial \rho'}{\partial y}\,dz + \frac{A_l}{gH}\int_0^H \frac{\partial^2 v}{\partial x^2}\,dz \tag{7}$$

By the same method we derive from equation (1) the equation for the zonal part of a solid boundary. The right side of equation (7) is considered to be known, because $\rho$ is specified and $v$ is taken into account by the method of successive approximation. Equation (7) enables us to calculate $\zeta$ on the solid side boundaries. The specific method of such calculations was given earlier (Sarkisyan, 1969, 1976).

We now have five equations (1)-(5) for the five unknown functions $u$, $v$, $w$, $p$, $\zeta$. The boundary conditions for these functions are also specified. Let us make a preliminary evaluation of terms on the right side of equation (7). For this reason we specify the characteristic horizontal and vertical scales respectively $L_0 = 10^7$ cm, $H_0 = 10^5$ cm. The characteristic density anomaly and flow velocity at the equatorial region are $(\delta\rho')_0 = 5 \times 10^{-4}$ g/cm$^3$, $V_0 = 50$ cm/s. Then characteristic values of the first and the second terms are respectively

$$\frac{(\delta\rho)_0 H_0}{2\rho_0 L_0} = 2.5 \times 10^{-6}$$

and

$$\frac{A_l V_0}{gL^2{}_0} = 5 \times 10^{-9}, \text{ if } A_l = 10^7 \text{cm}^2/\text{s}.$$

We see that the main term on the right side of (7) is the first term. Of course the second term could be larger if we were considering the small scale currents near the side boundaries, but it is not the subject of our investigation. For our purpose then, it is possible to take into account the second term by the method of successive approximation.

We calculate the components of horizontal velocity directly from equations of motion (1) and (2), the numerical scheme constructed on the basis of importance of the nonlinear terms. Two versions of numerical schemes have been performed in the calculations. We describe them here on the basis of equation (1). The first version is

$$-\frac{u^{(n)} - u^{(n-1)}}{\delta t} + A_l \nabla^2 u^{(n)} - u^{(n-1)}\frac{\partial u^{(n)}}{\partial x} - v^{(n-1)}\frac{\partial u^{(n)}}{\partial y} \tag{8}$$

$$= g\frac{\partial \zeta}{\partial x} + \frac{g}{\rho_0}\int_0^z \frac{\partial \rho'}{\partial x}\,d\xi - fv^{(n-1)} + w^{(n-1)}\frac{\partial u^{(n-1)}}{\partial z} - \frac{\partial}{\partial z}\,\nu\,\frac{\partial u^{(n-1)}}{\partial z}$$

$n$ and $\delta t$ being the number and the value of the time step.

The second version is

$$-\frac{u^{(n)}-u^{(n-1)}}{\delta t}+A_l\nabla^2 u^{(n)}-u^{(n-1)}\frac{\partial u^{(n)}}{\partial x}-v^{(n-1)}\frac{\partial u^{(n)}}{\partial y}+\frac{\partial}{\partial z}\,\nu\,\frac{\partial u^{(n)}}{\partial z}$$

$$-w^{(n-1)}\frac{\partial u^{(n)}}{\partial z}=g\frac{\partial \zeta}{\partial x}+\frac{g}{\rho_0}\int_0^z\frac{\partial \rho'}{\partial x}\,d\xi-fv^{(n-1)}\,. \tag{9}$$

where the terms $w\,\frac{\partial u}{\partial z}$ and $\frac{\partial}{\partial z}\,\nu\,\frac{\partial u}{\partial z}$ are treated implicitly and therefore put on the left-hand side.

The first version is useful only when the terms $w\,\frac{\partial u}{\partial z}$ and $\frac{\partial}{\partial z}\,\nu\,\frac{\partial u}{\partial z}$ are sufficiently small, otherwise, a large value of $A_l$ will be required for stability. Although the second version will remain stable for much larger values of $w\,\frac{\partial u}{\partial z}$ and $\frac{\partial}{\partial z}\,\nu\,\frac{\partial u}{\partial z}$, it requires more complex computer code. Experience with actual numerical experiments will indicate which method is preferable.

Equation (2) is transformed to the form (8) or (9) in the same manner. We see that a linearization (in a finite difference sense) was made when passing from equation (1) to equation (8) or (9), because the linear finite difference scheme allows economy in the computer's storage. The addition of the terms with time differences brings us to the initial value problem and so essentially simplifies the construction of a stable numerical scheme.

The preliminary calculations, made by scheme (8) but without first terms of the left part of this equation (Demin, 1975b) showed that the numerical scheme for (8) succeeded only with an overestimated value of $A_l > 10^9\text{cm}^2/\text{s}$. As for equation (5) for $\zeta$, its finite difference scheme possessed a large "reserve of stability," it succeeds with any small value of $A_l$ and does not need the addition of terms such as $\frac{\partial \zeta}{\partial t}$ or $\frac{\partial}{\partial t}\nabla^2\zeta$ .

By method of direct differences and using the above mentioned boundary condition, it is easy to transform the effect of the vertical turbulent viscosity on the sea surface in equations (8) and (9) to the form

$$\frac{\partial}{\partial z}\,\nu\,\frac{\partial u}{\partial z}\Big|_{z=0}\approx\frac{1}{z_1}\left(\frac{\tau_x}{\rho_0}+\nu\,\frac{\partial u}{\partial z}\Big|_{z=z_1}\right) \tag{10}$$

where $z_1$ is the depth of the shallowest level of the model. It is easy also to make a more decisive approximation of this term by expanding the term in a Taylor's series.

We obtained a formula for the vertical component of velocity by integrating the continuity equation and using the boundary condition $w|_{z=0}=0$:

$$w^{(n)} = -\int_0^z \left(\frac{\partial u^{(n)}}{\partial x} + \frac{\partial v^{(n)}}{\partial y}\right) d\xi \tag{11}$$

We now have all relations for calculation of the four functions $u$, $v$, $w$, and $\zeta$. The pressure field is calculated easily using formula (3). The relation (11) is also a simple formula; the main process of the numerical calculations is connected with equations for $u$, $v$, and $\zeta$. It is possible to present all three relations for these functions in a unified form. For simplicity we present this unified equation for the first numerical scheme:

$$\nabla^2 F^{(n)} - \frac{1-\delta_1}{A_l \delta t} F^{(n)} + C_1{}^{(n-1)} \frac{\partial F^{(n)}}{\partial x} + C_2{}^{(n-1)} \frac{\partial F^{(n)}}{\partial y} = G^{(n-1)} - \frac{1-\delta_1}{A_l \delta t} F^{(n-1)} \tag{12}$$

where $G = \Theta$, $\phi u/A_l$, $\phi v/A_l$ for $F = \zeta$, $u$, $v$ respectively. $\Theta$, $\phi u$, $\phi v$ are the right-hand sides of the $\zeta$, $u$ and $v$ equations; and

$$C_1{}^{(n-1)} = \frac{\delta_1}{H}\frac{\partial H}{\partial x} - (1-\delta_1)\frac{u^{(n-1)}}{A_l}\,; \quad C_2{}^{(n-1)} = \frac{\delta_1}{H}\frac{\partial H}{\partial y} - (1-\delta_1)\frac{v^{(n-1)}}{A_l}\,,$$

$\delta_1 = 1$ for the equation for $\zeta$, and $\delta_1 = 0$ for the $u$, $v$ equations.

A stable difference scheme with diagonal dominance is readily constructed with directed differences. For the regular grid interval in both $x$ and $y$ coordinates, the final form of the finite difference equation (12) is as follows:

$$\begin{aligned} F^{(n)}{}_{k,j,i} = \frac{1}{a_{k,j,i}{}^{(n-1)}} \Bigg\{ & \left[\frac{\delta y}{\delta x} + C_{1\,k,j,i}{}^{(n-1)}\,(m_1-1)\delta y\right] F_{k,j,i-1}{}^{n} \\ & + \left(\frac{\delta y}{\delta x} + C_{1k,j,i}{}^{(n-1)}\, m_1\, \delta y\right) F_{k,j,i+1}{}^{(n)} + \left[\frac{\delta x}{\delta y} + C_{2k,j,i}{}^{(n-1)}\,(m_2-1)\,\delta x\right] F_{k,j-1,i}{}^{(n)} \\ & + \left(\frac{\delta x}{\delta y} + C_{2k,j,i}{}^{(n-1)}\, m_2 \delta x\right) F_{k,j+1,i}{}^{(n)} - G_{k,j,i}{}^{(n-1)} + \frac{1-\delta 1}{A_l \delta t} F_{k,j,i}{}^{(n-1)} \Bigg\} \end{aligned} \tag{13}$$

where $k$, $j$, $i$ are grid point indices for the $z$, $y$, $x$ axes respectively, and $\delta x$, $\delta y$ are the grid intervals,

$$m_s = \begin{cases} 1, \text{ if } C_{s\,k,j,i}{}^{(n-1)} > 0 \\ 0, \text{ if } C_{s\,k,j,i}{}^{(n-1)} < 0, \end{cases} (s = 1,2)$$

$$C_{1k,j,i}{}^{(n-1)} = \frac{\delta_1}{H_{j,i}}\frac{H_{j,i+1} - H_{j,i-1}}{2\delta x} - (1-\delta_1)\frac{u_{k,j,i}{}^{(n-1)}}{A_l}\,;$$

$$C_{2k,j,i}{}^{(n-1)} = \frac{\delta_1}{H_{j,i}}\frac{H_{j+1,i} - H_{j-1,i}}{2\delta y} - (1-\delta_1)\frac{v_{k,j,i}{}^{(n-1)}}{A_l}\,;$$

$$\begin{aligned} a_{k,j,i}{}^{(n-1)} = {} & \frac{(1-\delta_1)\delta x \delta y}{A_l\,\delta t} + \frac{2\delta y}{\delta x} + \frac{2\delta x}{\delta y} + C_{1k,j,i}{}^{(n-1)}\,(2m_1-1)\,\delta y \\ & + C_{2k,j,i}{}^{(n-1)}\,(2m_2-1)\,\delta x. \end{aligned}$$

The differentials on the right sides of the equations are approximated by centered finite differences, and the integrals are calculated by the trapezoidal rule.

The implicit linear finite difference scheme of first order of approximation is used for the solution of the problem. Such a scheme does not make high demands on computer storage. The scheme is stable and very efficient, even when the value of $A_l$ is relatively small ($5 \times 10^7 \text{cm}^2/\text{s}$ for the first scheme and $10^6 \text{cm}^2/\text{s}$ for the second). The calculation is as follows: First, we make one inner iteration and calculate the first approximation $\zeta^{(1)}$ by given density $\rho'$ and wind stress $\tau_x$, $\tau_y$, using any initial fields for $\zeta$, $u$, $v$, $w$; then calculate the first approximation $u^{(1)}$, $v^{(1)}$ for all of the levels, using $\zeta^{(1)}$ and initial approximations for $u$, $v$, $w$. At last we calculate $w^{(1)}$, from $u^{(1)}$, $v^{(1)}$. Afterward we calculate the second approximation $\zeta^{(2)}$ in the same manner and so on. The calculations are carried out until steady state is reached. The criterion is max $(|u^{(n)} - u^{(n-1)}|, |v^{(n)} - v^{(n-1)}|) < \epsilon$. Practically, it is enough to put $\epsilon = 10^{-3} - 10^{-2} \text{cm/s}$.

### 3. The results of calculation

The calculations have been carried out for the equatorial belt of the Atlantic ocean situated between 3°N to 3°S and 32°W to 4°E. The density field used in these calculations was taken from data of the international program EQUALANT II for the levels of 0, 75, 100, 150, 200, 400, 600, 800, and 1000 m and the wind stress from the paper of Shalaveyus (1966). The grid of steps in the main numerical experiments was $\delta x = 2°$, $\delta y = 1°$. In some experiments the grid mesh $\delta y$ was made as small as 0.5°. The minimum value of the vertical mesh in the upper 100 m layer was 25 m. The density field had a mean value for each $2° \times 2°$ square, available for the region 11°N to 11°S. Earlier, the authors made calculations of the tropical region currents, using this density field (Demin and Sarkisyan, 1974, Demin, 1975a). The results of these calculations were used here as a boundary condition for $u$, $v$, and $\zeta$ on the northern and southern boundaries (3°N and 3°S). The meridional boundaries of the region considered are liquid, therefore we construct the necessary boundary values here by interpolation. The density field for the high resolution grid mesh was also obtained by interpolation, because we had no precise data. Because of the density field deficiencies we consider this work to have theoretical rather than oceanographic interest. The analysis of the relative role of hydrodynamic factors in this model is considered to be the main interest.

The optimal value of the time step was defined by test calculation $\delta t = 5 \times 10^4 s$. The spin-up process was controlled by the above mentioned criterion and by the behavior of mean kinetic energy.

The time for spin-up equals one to three months depending on initial approximation and parameter values. The final results do not depend on the initial approximation. The greater part of the calculations were carried out by the second numerical scheme, the reason for which will be seen later.

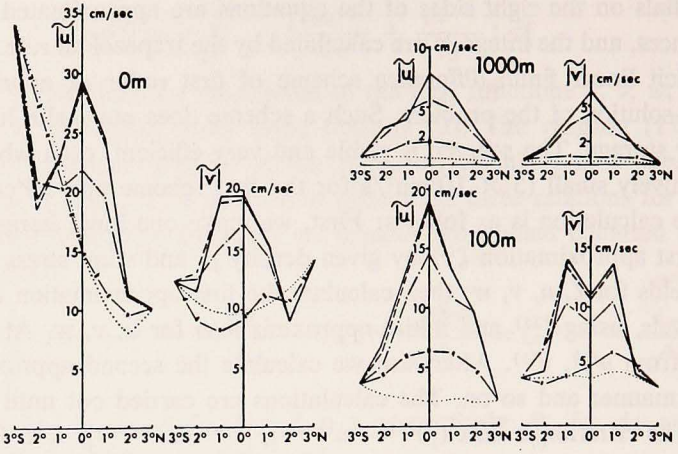


Figure 1. The zonal mean intensity of currents for different values of $A_l$ at the depth of 0, 100 and 1000 meters. Full lines correspond to $A_l = 10^6 cm^2/s$, – – – – – – to $A_l = 10^7$, –•–•– to $A_l = 10^8$, –||–||–||– to $A_l = 10^9$, • • • • to $Al = 10^{10}$.

The first calculation series was carried out for the grid steps $\delta x = 2°$, $\delta y = 1°$ and parameters $\nu = 10$ cm²/s, $\rho_0 = 1.028$ cm²/s, the value of $A_l$ varying between $10^{10}$ and $10^6$ cm²/s. The dependence of the solution on the value of $A_l$ is illustrated in Figure 1. The solution is highly smoothed and there is practically no equatorial intensification when $A_l$ is as large as $10^9 - 10^{10}$ cm²/s. Table 1 shows that the

Table 1. The "weights" of the nonlinear and turbulent terms in the equations (1) and (2) (absolute values in relative units of the latitudinal mean and average for the whole region). The upper figures correspond to $A_l = 10^9$ cm²/s and the lower ones—to $A_l = 10^7$ cm²/s; a) at the seasurface, b) at the depth of 400 m.

Table 1a.

0 m

| Latitude | $A_l \Delta u$ | $A_l \Delta v$ | $u \frac{\partial u}{\partial x}$ | $u \frac{\partial v}{\partial x}$ | $v \frac{\partial u}{\partial y}$ | $v \frac{\partial v}{\partial y}$ | $\frac{\partial}{\partial z} \nu \frac{\partial u}{\partial z}$ | $\frac{\partial}{\partial z} \nu \frac{\partial v}{\partial z}$ |
|---|---|---|---|---|---|---|---|---|
| 2°S | 158 | 613 | 62 | 84 | 55 | 76 | 463 | 666 |
| | 19 | 15 | 43 | 64 | 219 | 157 | 472 | 667 |
| 1° | 194 | 295 | 34 | 43 | 42 | 43 | 268 | 519 |
| | 11 | 22 | 103 | 81 | 279 | 274 | 271 | 523 |
| 0° | 234 | 345 | 28 | 23 | 45 | 34 | 213 | 558 |
| | 20 | 19 | 180 | 85 | 131 | 354 | 214 | 557 |
| 1° | 236 | 358 | 24 | 16 | 87 | 63 | 246 | 592 |
| | 17 | 21 | 105 | 67 | 280 | 241 | 242 | 590 |
| 2°N | 348 | 409 | 18 | 16 | 98 | 64 | 290 | 664 |
| | 13 | 13 | 28 | 41 | 256 | 101 | 291 | 660 |
| average | 234 | 404 | 33 | 36 | 66 | 56 | 296 | 600 |
| | 16 | 18 | 94 | 67 | 233 | 226 | 298 | 601 |

Table 1b.

400 m

| Latitude | $A_t \Delta u$ | $A_t \Delta v$ | $u \frac{\partial u}{\partial x}$ | $u \frac{\partial v}{\partial x}$ | $v \frac{\partial u}{\partial y}$ | $v \frac{\partial v}{\partial y}$ | $\frac{\partial}{\partial z}$ | $v \frac{\partial u}{\partial z}$ | $\frac{\partial}{\partial z}$ | $v \frac{\partial v}{\partial z}$ | $w \frac{\partial u}{\partial z}$ | $w \frac{\partial v}{\partial z}$ |
|---|---|---|---|---|---|---|---|---|---|---|---|---|
| 2°S | 108 | 153 | 6 | 2 | 4 | 7 | | 0.4 | | 0.4 | 2 | 1 |
| | 6 | 3 | 7 | 7 | 25 | 8 | | 0.3 | | 0.6 | 5 | 11 |
| 1° | 146 | 115 | 5 | 4 | 5 | 7 | | 0.4 | | 0.8 | 7 | 3 |
| | 8 | 9 | 16 | 23 | 26 | 58 | | 0.5 | | 1.1 | 55 | 36 |
| 0° | 142 | 193 | 6 | 5 | 5 | 11 | | 0.5 | | 0.9 | 9 | 7 |
| | 16 | 13 | 41 | 34 | 75 | 119 | | 1.0 | | 0.7 | 107 | 68 |
| 1° | 126 | 155 | 5 | 5 | 7 | 4 | | 0.7 | | 0.8 | 5 | 6 |
| | 7 | 16 | 26 | 15 | 124 | 78 | | 1.0 | | 1.0 | 42 | 43 |
| 2°N | 98 | 193 | 3 | 3 | 5 | 6 | | 0.7 | | 0.5 | 3 | 3 |
| | 6 | 5 | 10 | 6 | 18 | 26 | | 1.0 | | 0.6 | 20 | 13 |
| average | 124 | 162 | 4 | 4 | 5 | 7 | | 0.5 | | 0.7 | 5 | 4 |
| | 9 | 9 | 20 | 17 | 53 | 58 | | 0.8 | | 0.8 | 46 | 34 |

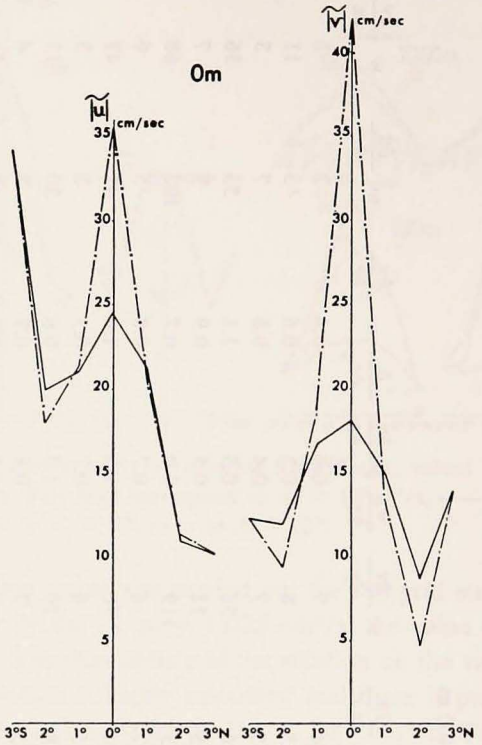
0m
cm/sec
40
35
30
25
20
15
10
5
3°S 2° 1° 0° 1° 2° 3°N

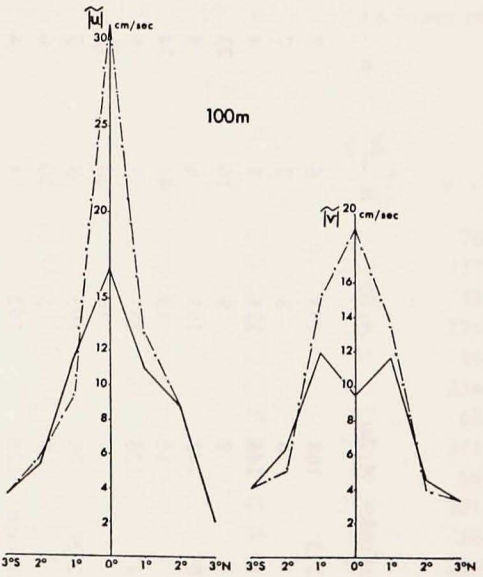
100m
cm/sec
30
25
20
15
12
10
8
6
4
2
3°S 2° 1° 0° 1° 2° 3°N

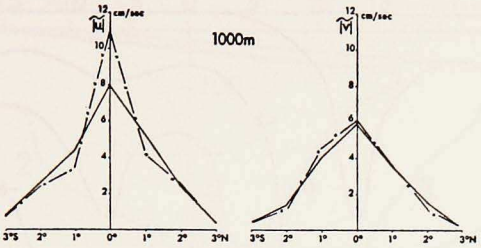


Figure 2. The zonal mean intensity of currents for the nonlinear (full lines) and linear (broken lines) versions to the depth of 0(a), 100(b) and 1000(c) meters for $A_l = 5 \times 10^7 \text{cm}^2/\text{s}$.

effect of horizontal momentum diffusion is one order greater than the nonlinear terms when $A_l = 10^9$ cm$^2$/s. Actually in the case of such a large value $A_l$ one deals with an essentially linear problem. We claim that the value of $A_l$ has to be sufficiently small so as not to suppress the nonlinear terms. At best the solution is controlled greatly by boundary conditions, if $A_l$ is as large as $10^9 - 10^{10}$ cm$^2$/s.

We have other results when $A_l$ equals or is less than $10^8$ cm$^2$/s. In these cases we have clearly expressed the equatorial peak of intensity of zonal currents, and, in intermediate levels (75-200m), there is an equatorial minimum of meridional currents. The effect of nonlinear terms is essential now. For example, when $A_l = 10^7$ cm$^2$/s, the average value of nonlinear terms is one order greater than the effect of horizontal turbulence (see Table 1). The "weight" of almost all the nonlinear terms is growing from the northern and southern boundary regions toward the equator. There is practically no such effect for the large values of $A_l$. At last the solution does not depend so much on boundary conditions for the small $A_l$. Further decreasing of $A_l$ below $10^7$ cm$^2$/s practically does not affect the calculation results. Let us note that the numerical viscosity is predominant, when $A_l$ is too small. Therefore the question arises how much is the numerical viscosity. For the first rough estimation we obtain the value of the order of the viscosity coefficient $A_{\text{num}} \approx \frac{uh}{2}$ to be between $10^7$ and $10^8$ cm$^2$/s. But the essential differences of the calculation results obtained for $A_l = 5 \times 10^7$ cm$^2$/s and $A_l = 10^7$ cm$^2$/s indicate that the effective value of $A_{\text{num}}$ is nearly $10^7$ cm$^2$/s. The most important is that the numerical viscosity is not so much as to suppress the nonlinear terms. This conclusion will be confirmed below, when discussing the additional calculation results.

To make a clearer comparison with general nonlinear versions, we performed a full linear version of the problem (the nonlinear terms were excluded both in the equations of motion and in the equation for $\zeta$). When $A_l \geqslant 10^9$ cm$^2$/s the results are practically the same. The difference between the two versions increases (especially at the equator) when decreasing the value of $A_l$, and becomes very pronounced for the $A_l = 5 \times 10^7$ cm$^2$/s (Fig. 2a,b,c). In the linear version the inten-

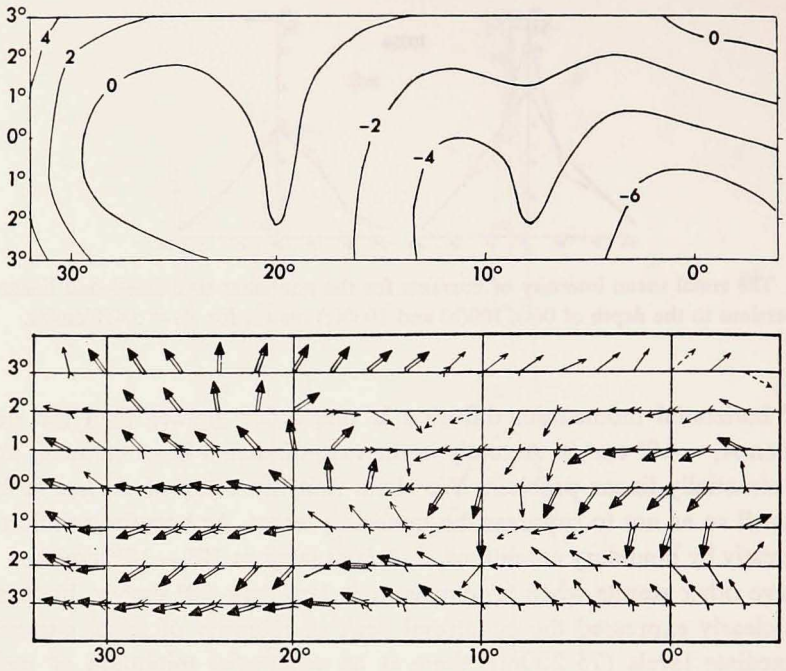


Figure 3. The water circulation in the equatorial region.

a) sea surface topography in cm.

b) sea-surface currents (•••> ≤2 cm/s, ------→ 3-5, ⟶ 6-10, >⟶ 11-15, ≫⟶ 16-20, ⟹ 21-30, >⟹ 31-50, ≫⟹ 51-75).

c) the vertical profiles of the current's zonal component at four points of the equator 1-30°W, 2-20°W, 3-14°W, 4-4°W.

sity of the meridional component of the sea surface currents is larger than the zonal one, and it is an unrealistic result. Also, the meridional drag of velocity seems to be too large, and in the intermediate levels we have equatorial maximum of the meridional velocity component instead of minimum. It is interesting to note that the difference between linear and nonlinear versions is larger in the eastern part of the basin, where the density field is less smooth. On the whole, the difference between the two versions increases toward the equator and decreases with depth. In the upper layer the "weight" of the terms $v\frac{\partial v}{\partial y}$, $v\frac{\partial u}{\partial y}$ is the largest in comparison with other nonlinear terms. The values of these terms decrease with depth, and at the levels where $z > 75$ m, the terms $w\frac{\partial u}{\partial z}$, $w\frac{\partial v}{\partial z}$ become quite sufficient. We should mention here that the importance of the nonlinear effects in the undercurrent region was shown by Knauss (1966) masked on the observational data. Gill (1975) has

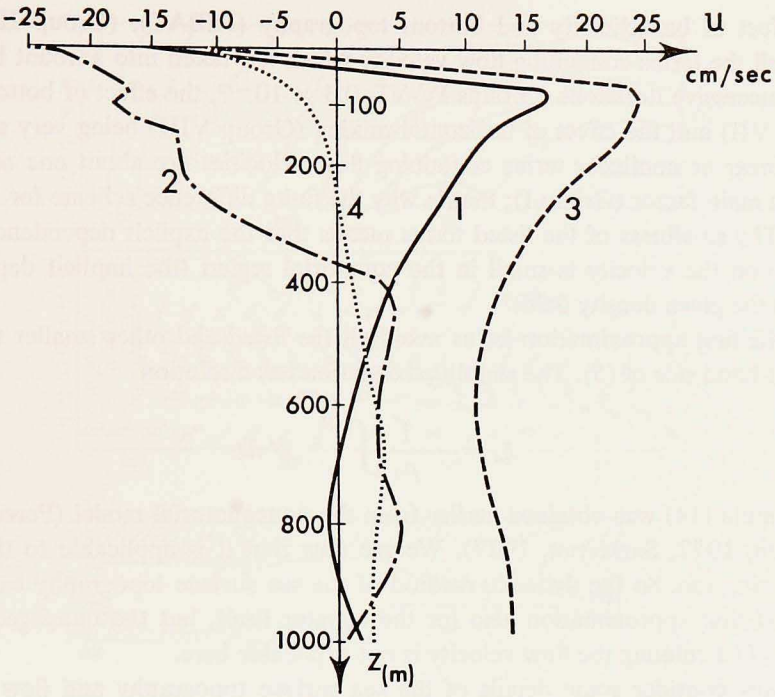


analyzed simplified models of the equatorial currents and discussed the possible physical reasons for the nonlinear equatorial intensification of the zonal flow.

Short notes on the role of other factors (for the case of $\nu = 10$ cm$^2$/s, $A_l = 5 \times 10^7$ cm$^2$/s): The importance of $\tau_x$ and $\tau_y$ for determining the surface currents is obvious. When excluding this factor, the meridional component of the surface gradient current becomes larger. The direct wind stress effect decreases with depth and becomes unimportant at the level of $z = 100$ m. The role of the vertical turbulence itself becomes small at the levels $z = 150$-$200$ m if $\nu = \text{const}$. At a distance of 1° from the equator, the Coriolis acceleration effect is so important that it is impossible to exclude it even in the case of investigation of currents in a narrow equatorial belt. The role of the bottom relief is relatively small. In the case of a flat bottom ocean ($H = 4$ km), the mean relative difference of current velocity from the main version is only 2-4% at the sea surface, and about 10% at a depth of 1000 m.

In the versions listed above, the sea surface topography does not change much in spite of essential alterations of the flow velocity. The balance of the forces in equation (5) is the cause of such differences between the behavior of $\zeta$ and flow dynamics in the equatorial currents system. The absolute mean values of the terms of the right side of equation (5) are as follows (in CGS units): Direct wind stress (Group III) $2 \times 10^{-17}$, the main effect of baroclinicity (Group I) $3.2 \times 10^{-15}$, the

joint effect of baroclinicity and bottom topography (JEBAT), (Group II) $0.3 \times 10^{-15}$, all the terms containing flow velocity which are taken into account by methods of successive iterations (Groups IV-VI) $0.3 \times 10^{-15}$, the effect of bottom stress (Group VII) and the effect of horizontal mixing (Group VIII) being very small. So either linear or nonlinear terms containing flow velocities are about one order less than the main factor (Group I); that is why the finite difference scheme for $\zeta$ is very stable. The smallness of the listed terms means that the explicit dependence of the pressure on the velocity is small in the equatorial region (the implicit dependence exists in the given density field).

For the first approximation let us avoid all the listed and other smaller terms on the right-hand side of (5). The simplified equation has a solution

$$\zeta_a = -\frac{1}{\rho_0}\int_0^H \rho' \, dz \tag{14}$$

The formula (14) was obtained earlier from the nonequatorial model (Peredery and Sarkisyan, 1972; Sarkisyan, 1977). We see now that it is applicable to the equatorial region too. So the dynamic method of the sea surface topography calculation is a good first approximation also for the equator itself, but the quasi-geostrophic method of calculating the flow velocity is not applicable here.

We now consider some details of the sea surface topography and flow velocity in the region. The sea surface maximum displacement is not large here; it equals only 13 cm. The general west-east slope was obtained correctly, but as shown on Figure 3a, this slope is not regular. The sea surface currents are formed mainly by trade winds and are directed from east to west. The maximum flow velocity equals 74 cm/s, its average being about 30 cm/s. The equatorial divergence is clearly shown in the western part of the region (Fig. 3b).

The velocity, as a rule, reverses its direction with depth because the wind drift decreases rapidly, and the predominant slope generates eastward currents at the equator (Fig. 3c). But as a result of irregularity of the sea surface slope, the undercurrent does not exist everywhere; there are regions of stream "discontinuity," and vortices exist there. Therefore, the question arises, is this undercurrent irregular because of the specified density field, or is it the peculiarity of the model? To answer this question, one could make numerical experiments with different versions of a smoothed density field. We chose other ways here, because we know it is easy to prepare the density field which would express any known gradient current. The experiment that was made is as follows:

The equatorial region was made homogeneous ($\rho' = 0$). However, the boundary conditions for the sea surface topography were retained from the previous model. That is, the sea surface along the liquid boundaries was prescribed from the quasi-geostrophic, baroclinic, extraequatorial model. We obtained a regular west-east sea surface slope (Fig. 4a) and, as a result, a clearly defined continuous under-

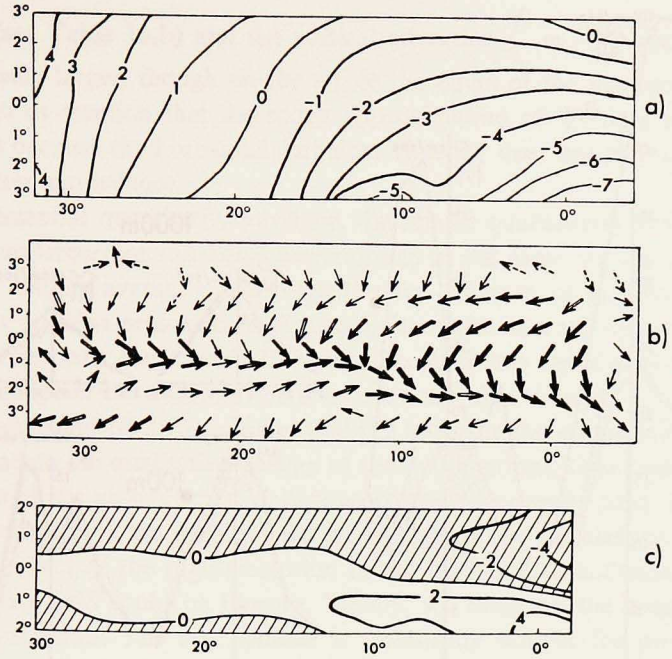


Figure 4. The current velocities for an idealized model version ($\rho = 0$ in the interior of the basin, with baroclinic boundary condition on side boundaries).

a) sea-surface topography in cm

b) currents at $z = 75$m ( ----→ ≦ 5 cm/s, ——→ 6-15, ⟹ 16-25, ▬→ 26-50).

c) vertical velocity field at $z = 200$ m, isolines interval equal to $2 \times 10^{-3}$cm/s, upwelling regions are dotted.

current (Fig. 4b). This undercurrent is convergent; thus there is an equatorial belt of downwelling, surrounded by upwelling regions on the north and south (Fig. 4c).

In the upper layer a region of upwelling predominates, connected with divergence of the equatorial trade wind currents. This artificial version is used only to test the model. We do not consider the full homogeneous ocean model (including boundary conditions), because in this case the sea surface slope and gradient flow velocities would be unrealistically small. By our earlier experiment, the maximum amplitude of $\zeta$ in the latitude range 11°S-11°N for the homogeneous ocean was equal to 0.8 cm (Demin and Sarkisyan, 1974).

In the above mentioned baroclinic versions sea surface anomalies are determined mainly by the first term of the right-hand side of equation (5), i.e. mainly by the equatorial water baroclinicity. As for this special case, the right-hand side is very small ($\rho \equiv 0$) and the solution is determined mainly by the baroclinic boundary conditions. So the undercurrent in this case is mainly generated by the extraequatorial water mass baroclinicity.

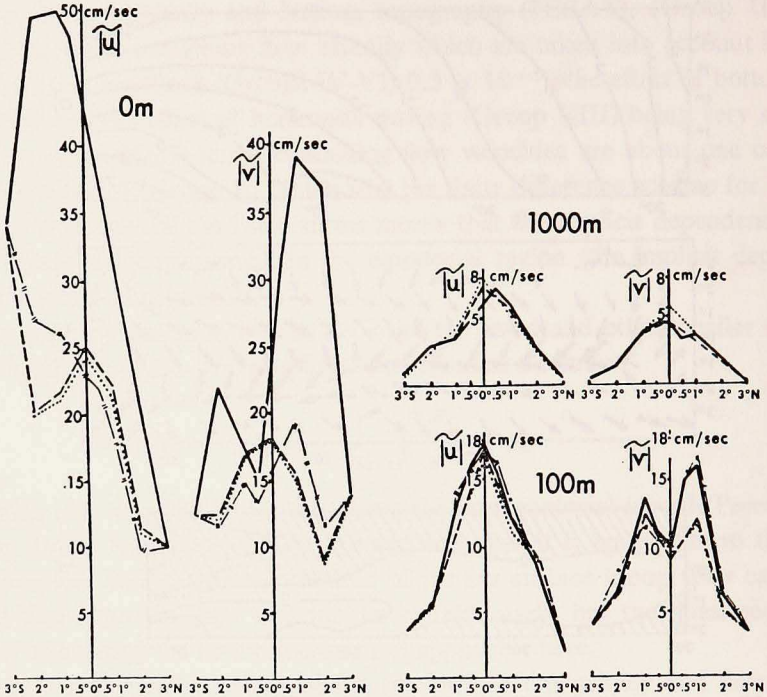


Figure 5. The zonal mean intensity of currents for different versions of the model and different resolutions for $A_t = 5 \times 10^7$ cm²/s; Full lines = the second scheme, high resolution, $\nu$ = 10 cm²/s; –||–||– The second scheme, high resolution, $\nu = 10^2$ cm²/s; • • • • The first scheme, coarse resolution, $\nu$ = 10 cm²/s; – – – The second scheme, coarse resolution, $\nu$ = 10 cm²/s.

An additional numerical experiment was carried out with high resolution. In this case the meridional grid step was equal to 0.5°, the minimal vertical grid step equal to 25 m (in upper 100 meters). The basic density field was interpolated to this irregular grid. The result is presented in Fig. 5. We can see that the sea surface current is much more intense. There are more points now with westward currents. It is interesting to note that the local minimum of the meridional current component appeared at the sea surface as well. This minimum is shifted 0.5° from the equator and may be because the horizontal grid step is still large. The differences between the fine and coarse resolutions decrease with depth and at the level of 100 m are relatively small. We found that the main differences are due to splitting of the vertical grid mesh. The sea surface and deeper layer currents depend differently on the grid resolution, because the balance in momentum equatorial depends on depth. In the surface layer the vertical turbulent viscosity and the horizontal momentum advection $\left( \nu \frac{\partial u}{\partial y} \text{ and } \nu \frac{\partial v}{\partial y} \right)$ are essential. In the deeper layer the vertical viscosity

is very small (see Table 1a,b) and the vertical advection $\left( w \frac{\partial u}{\partial z} \text{ and } w \frac{\partial v}{\partial z} \right)$ becomes relatively larger, though on the whole the effect of the nonlinearity fades with depth. Let us mention that the rough approximation of $\nabla^2$ does not lead to essential errors because the horizontal turbulent viscosity does not play an essential role in the momentum balance.

In spite of essential quantitative variance, the results qualitatively are the same. The jet of the undercurrent still has a discontinuity at the same regions considered. The curves of zonally averaged flow velocities for the case of an over-estimated $\nu = 100$ cm$^2$/s are also presented in Figure 5. It results in a strong smoothing of the sea surface currents. But even in this case, the difference rapidly decreases with depth, and the shape of the undercurrent does not noticeably change.

So, the improvement of the resolution and the interpolation of the initial density field did not lead to the qualitative change of the undercurrent. One could obtain a detailed picture of the undercurrent only from the precise density field. Because of the decisive character of the density field we did not make calculations with high resolution. The effect of the high resolution in the diagnostic calculations with the inaccurate density field could be illusory. Finally, we dwell on the comparison of two numerical schemes. The first scheme is technically simpler for programming because it does not need a large computer storage. But as it appears now, it makes high demands on the original parameters, especially on $A_l$. The results of the calculations using both schemes are presented in Figure 5. They are near each other in the upper layers. The difference in lower layers is due to diverse methods of approximation of the terms $w \frac{\partial u}{\partial z}$, $w \frac{\partial v}{\partial z}$ because the role of these terms increases with depth. The calculation also shows that the spin-up time is less for the second method.

For these reasons almost all the presented calculations were done by the second scheme, and we recommend it for future calculations. This method can be easily transformed into the method of second order approximation in the horizontal by the technique given in Marchuk (1973) and Sarkisyan (1977).

## 4. Conclusions

1. The balance equation (5) seems to be very useful for equatorial region pressure anomaly calculations. The dynamic method of sea surface topography calculation by formula (14) is applicable for equatorial regions too.
2. The second version of the numerical method considered makes it possible to calculate equatorial currents and does not suppress the effect of nonlinear terms.
3. In any calculations of the equatorial currents the horizontal grid mesh in the meridional direction has to be no more than 0.5°, the vertical grid mesh in upper 100-150 meters has to be no more than 25 m and the coefficient of horizontal vis-

cosity (turbulent or numerical) has to be no more than $10^7 cm^2/s$. Otherwise, the nonlinear terms are being suppressed by overestimating horizontal mixing.

4. The density field is the main indicator of equatorial gradient currents; moreover this field has to be more accurate here than in nonequatorial regions. The wind stress is important for calculation of the sea surface currents, but its effect fades with depth and becomes unimportant at the level of 100-150 m.

*Acknowledgment.* In spring of 1976 this paper was discussed at the seminars of GFDL of Princeton University and at Yale University. The authors are grateful to George Veronis, Kirk Bryan and other colleagues for their helpful comments.

## REFERENCES

Bulatov, R. P., Yu. L. Demin, S. G. Poyarkov. 1975. Surface topography of the Atlantic Ocean. *Okeanologia,* N. *6,* 995–1001.

Cox, M. D. 1975. A baroclinic numerical model of the world ocean: preliminary results. Numerical Models of Ocean Circulation. Proceedings Symposium held in Durham, N. H., Oct. 17-20, 1972. National Academy of Sciences, Washington, D.C.

Demin, Yu. L., A. S. Sarkisyan. 1974. On the calculation of currents in a basin comprising the equator. *Izv. Acad. Nauk* SSSR, Fiz. Atmos. i Okeana. 10(11), 1194–1207.

Demin, Yu. L. 1975a. A diagnostic calculation of currents in the Tropical Atlantic. *Meteorologia i Hydrologia, 1,* 48–57.

—— 1975b. A nonlinear baroclinic model and calculation of currents in Equatorial Atlantic. *Izv. Akad. Nauk* SSSR, Fiz. Atmos. i Okeana. 11(5), 534–537.

Gill, A. E. 1975. Models of equatorial currents, *in* Numerical Models of Ocean Circulation, Nat. Acad. of Sci., Washington, D.C., 181–204.

Holland, W. R., A. D. Hirschman. 1972. A numerical calculation of the circulation in the North Atlantic Ocean. *Phys. Oceanogr., 2,* 336–354.

Knauss, I. A. 1966. Further measurements and observations of the Cromwell current. J. Mar. Res., *24,* 205–240.

Marchuk, G. I. 1973. Methods of Numerical Mathematics. Publishing House "Nauka," Siberian Branch, Novosibirsk.

Perederey, A. I. and A. S. Sarkisyan. 1972. Exact solutions of certain transformed dynamic equations of ocean currents. *Izv. Acad. Nauk* SSSR, Fiz. Atmos. i Okeana., *10,* 1073–1079.

Sarkisyan, A. S. 1969. Theory and calculations of ocean currents. Translation available from U. S. Department of Commerce and The National Science Foundation, Washington, D.C.

—— 1970. The theoretical models for calculation of currents in an oceanic basin, including the equator. Morskie Hydrofis. Issled. *2* MGI *Akad. Nauk* Ukr. SSR, Sevastopol.

—— 1977. The diagnostic calculations of a large-scale oceanic circulation, *in* The Sea, v. *VI,* Ch. 9, E. D. Goldberg, ed., New York, John Wiley & Sons.

Sarkisyan, A. S., A. F. Pastuchov. 1970. The density field as the main indicator of steady sea currents. *Izv. Acad. Nauk* SSSR, Fiz. Atmos. i Okeana, *6,* 64–76.

Sarkisyan, A. S., A. A. Serebryakov. 1974. On some results of the diagnostic calculations of the equatorial currents. Morskie Hydrofiz. Issled., *3,* MGI *Akad. Nauk Ukr.* SSR, Sevastopol.

Seidov, D. G. 1975. A calculation of hydrodynamic characteristics in the Gulf Stream region by given density field. *Izv. Akad. Nauk* SSSR, Fiz. Atmos. i Okeana, *11,* 93–95.

Shalaveyus, A. S. 1966. The wind field and wind stress in the equatorial region of the Atlantic ocean. Coll. papers: The Lomonosov Current. Kiev, Naukova Dumka, 141–153.

Received: *15 June, 1976;* revised: *3 January, 1977.*